



Contents lists available at ScienceDirect

Spectrochimica Acta Part A: Molecular and Biomolecular Spectroscopy

journal homepage: www.elsevier.com/locate/saa

Selective coordination ability of sulfamethazine Schiff-base ligand towards copper(II): Molecular structures, spectral and SAR study



Ahmed M. Mansour*

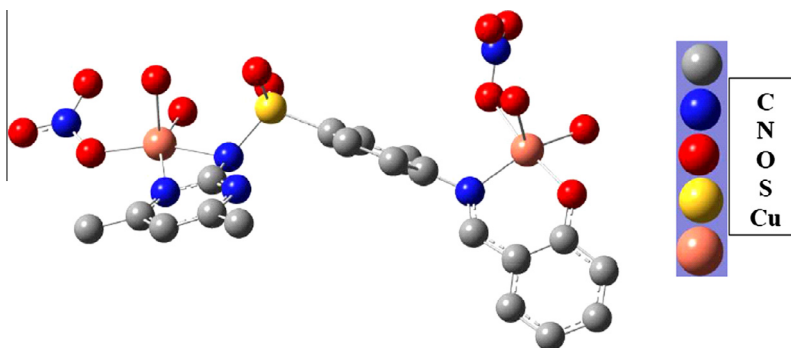
Chemistry Department, Faculty of Science, Cairo University, Gamaa Street, Giza 12613, Egypt

HIGHLIGHTS

- New mono- and binuclear Cu^{II} complexes of a sulfamethazine Schiff-base were prepared.
- Correlation between the experimental and theoretical work was performed.
- Mononuclear complex is less toxic than free ligand, while the binuclear one is inactive.
- E_{LUMO} , ΔE , dipole moment and polarizability correlate well with experimental LC_{50} .

GRAPHICAL ABSTRACT

Schiff-base derivative of established drug sulfamethazine has two different binding sites for copper(II) and show antibacterial activity in some cases.



ARTICLE INFO

Article history:

Received 8 August 2013
 Received in revised form 28 November 2013
 Accepted 8 December 2013
 Available online 18 December 2013

Keywords:

Copper complexes
 Schiff-base ligand
 EPR
 DFT
 Antibacterial activity
 Sulfamethazine

ABSTRACT

In the present work, a combined experimental and theoretical study of the N-(4,6-Dimethyl-pyrimidin-2-yl)-4-[(2-hydroxy-benzylidene)amino]benzenesulfonamide ligand (H_2L) and its mononuclear and magnetically diluted binuclear Cu^{II} complexes has been performed using IR, TG/DTA, magnetic, EPR, and conductivity measurements. Calculated g -tensor values showed best agreement with experimental values from EPR when carried out using the MPW1PW91 functional. Coordination of H_2L to a Cu^{II} center, regardless of the binding site and $\text{Cu}:\text{L}$ stoichiometry, leads to a significant decrease in the antibacterial activity compared to the free ligand as well as reference drugs in the case of *Staphylococcus aureus*. Structural-activity relationship suggests that E_{LUMO} , ΔE , dipole moment, polarizability and electrophilicity index were the most significant descriptors for the correlation with the antibacterial activity.

© 2013 Elsevier B.V. All rights reserved.

Introduction

Since their discovery, sulfonamides have been widely used for prophylaxis and treatment of bacterial infections [1] although they are bacteriostatic rather than bactericidal. Their value lies in the ability to slow down or prevent growth in wounds or infected

organs without appreciable toxicity to normal tissues [2]. However, several problems of sulfonamide therapy [3], include increasing bacterial resistance, adverse side-effects, and low bioavailability, were discovered. To tackle these problems, sulfonamides have been modified to coordinate to transition metal centers, for example by Schiff-base formation [4,5]. Such sulfonamides metal complexes now constitute an important field in bioinorganic chemistry [6,7]. For example, zinc-sulfadiazine [6] was used to prevent bacterial infections in animals suffering from burns.

* Tel.: +20 2 01222211253; fax: +20 2 35728843.

E-mail addresses: inorganic_am@yahoo.com, mansour@sci.cu.edu.eg

Sulfamethazine is a sulfa-based drug used as an antibacterial agent to treat livestock diseases [8]. As well as other sulfonamides, it has been modified by Schiff-base formation [4] and complexation to transition metals [9–11]. The titled ligand show a variable coordination mode depending on the reaction conditions and both $\text{Cu}(\text{HL})\text{X}$ and Cu_2LX ($\text{X} = \text{CH}_3\text{COO}^-$ and Cl^-) complexes could be isolated and studied [5]. Schiff-base derivatives of H_2L substituted in the 4- or 5-position of the salicylaldehyde residue by bromide or chloride were investigated for their chelation and biological properties [12,13]. In the present paper, the selective synthesis and characterization of a sulfamethazine-derived Schiff-base ligand H_2L (Fig. 1) and its mononuclear and binuclear $\text{Cu}(\text{II})$ complexes (Fig. 2) are reported to assist in the understanding of the

modulation of the antibacterial behavior of sulfamethazine upon modification and coordination to transition metals. Structural, electronic, spectroscopic and thermodynamic properties have been studied both experimentally and theoretically and are correlated here [14,15]. Structure–activity relationships (SAR) were used to correlate biological activity with some appropriate quantum descriptors [4,9] such as E_{HOMO} , dipole moment and molecular electrostatic potential.

Experimental

Synthesis of complexes

The ligand H_2L , and three novel mono- and binuclear copper(II) complexes **1–3** were synthesized as shown in Scheme 1.

Complex 1

Sodium sulfamethazine (300 mg, 1 mmol) in water (10 mL) was added to a solution of salicylaldehyde (122 mg, 1 mmol) in ethanol (20 mL) and heated to reflux for 4 h. Then, solid copper(II) nitrate trihydrate (242 mg, 1 mmol) was added and reflux continue for 1 h, whereupon the complex precipitated as a green solid. Yield: 67%. Anal. %Calcd. (%found). C, 39.41 (38.80); H, 4.35 (4.18); Cu, 10.97 (10.78); N, 12.09 (12.02). UV–Vis. (DMF): 278, 357, and

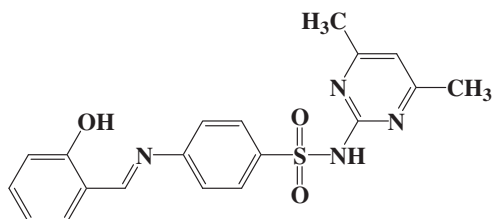


Fig. 1. Structure of ligand H_2L utilized in this work.

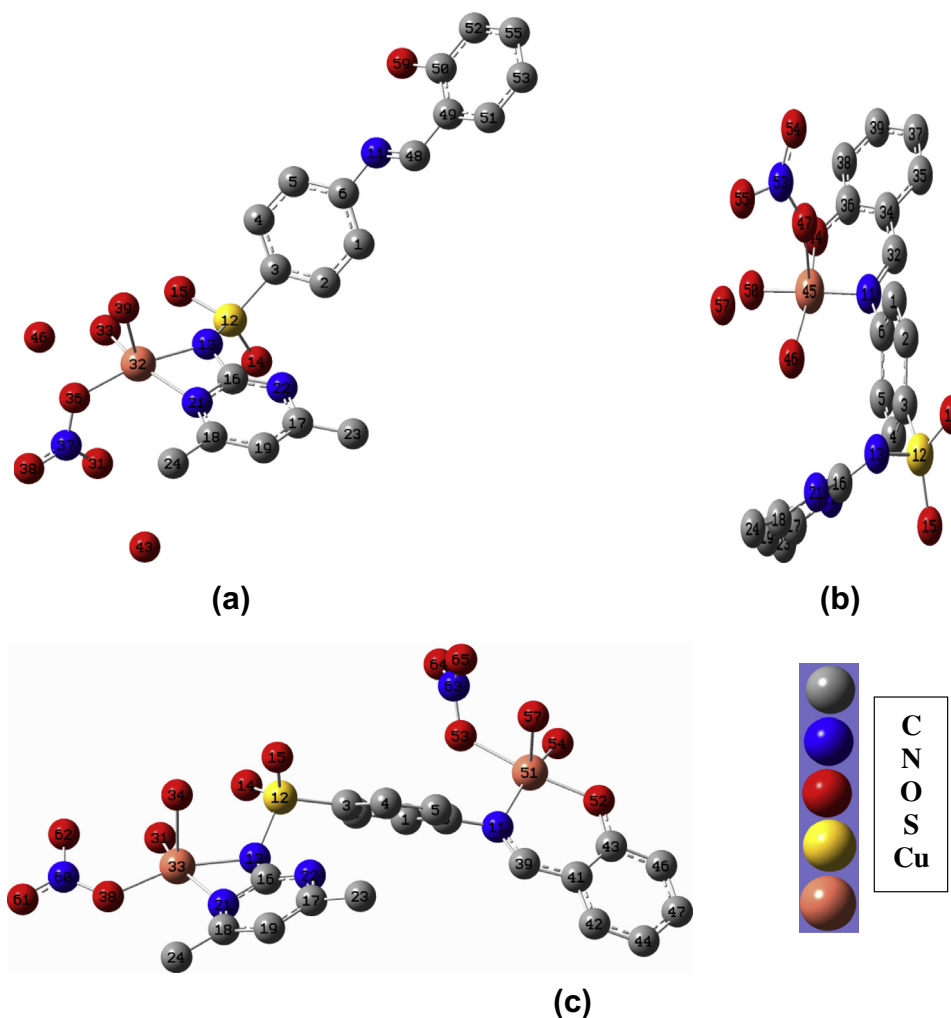
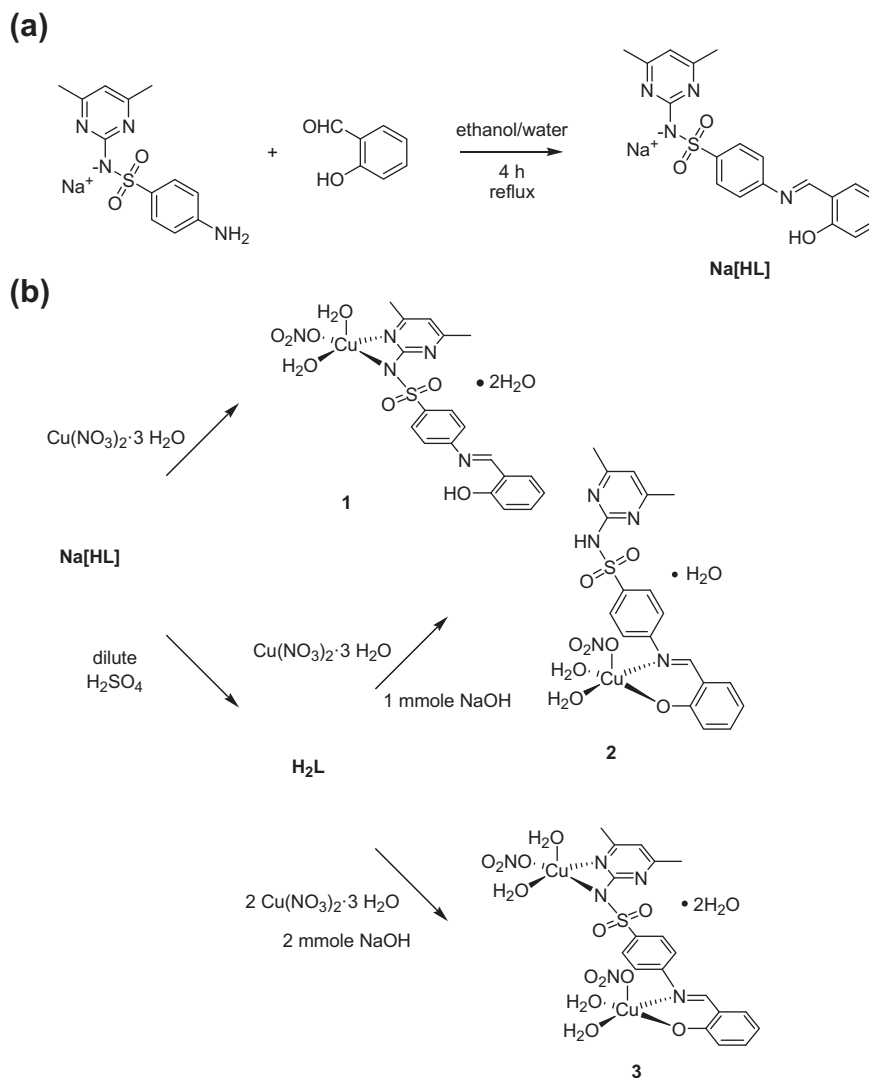


Fig. 2. Local minimum structures of complexes (a) **1**, (b) **2**, and (c) **3** obtained at the B3LYP/LANL2DZ level of theory.



Scheme 1. Synthesis of (a) **Na[HL]** and (b) its mono- and binuclear copper(II) complexes **1–3**.

454 nm. Molar Cond. (10^{-3} M, DMF): $17.30 \Omega^{-1} \text{ cm}^2 \text{ mol}^{-1}$. $\mu_{\text{eff}} = 1.70\mu_{\text{B}}$ (298 K).

Complex 2

Ligand **H₂L** was synthesized as previously reported [4]. An aqueous solution of **Na[HL]** (1 mmol, 15 mL, pH 7.5) was prepared using aqueous sodium hydroxide solution (40 mg, 1 mmol, 5 mL). Then, solid copper(II) nitrate trihydrate (242 mg, 1 mmol) was added and the solution heated to reflux for 2 h, whereupon the complex precipitated as a brown solid. Yield: 55%. Anal. %Calcd. (%found). C, 40.68 (40.62); H, 4.13 (4.04); Cu, 11.33 (11.17); N, 12.48 (11.63). UV–Vis. (DMF): 277, 355, and 464 nm. Molar Cond. (10^{-3} M, DMF): $17.75 \Omega^{-1} \text{ cm}^2 \text{ mole}^{-1}$. $\mu_{\text{eff}} = 1.75\mu_{\text{B}}$ (298 K).

Complex 3

Sodium hydroxide (80 mg, 2 mmol) was added to a suspension of ligand **H₂L** (381 mg, 1 mmol) in water (15 mL). Then, solid copper(II) nitrate trihydrate (500 mg, 2.05 mmol) was added and the solution heated to reflux for 2 h, whereupon the complex precipitated as a deep green solid. Yield: 72%. Anal. %Calcd. (%found). C, 30.85 (30.63); H, 3.82 (3.71); Cu, 17.18 (16.98); N, 11.36 (11.28). UV–Vis. (DMF): 277, 357, and 413 nm. Molar Cond. (10^{-3} M, DMF): $17.23 \Omega^{-1} \text{ cm}^2 \text{ mole}^{-1}$. $\mu_{\text{eff}} = 3.17\mu_{\text{B}}$ (298 K). The low molar conductance values indicate the non-electrolytic nature of

complexes **1–3**. Single crystals could not be obtained since the complexes only form amorphous materials as revealed by their XRD patterns.

Physical measurements

FT IR spectra were recorded as potassium bromide pellets using a Jasco FTIR 460 plus in the range of $4000\text{--}200 \text{ cm}^{-1}$. UV/Vis spectra were recorded on a Shimadzu Lambda 4B spectrophotometer. X-band EPR measurements were performed on solid samples at 298 K using a Bruker EMX spectrometer. The magnetic modulation frequency was 100 kHz and the microwave power was set to 0.201 mW. The *g*-values were obtained by referencing to a diphenylpicrylhydrazyl (DPPH) sample with *g* = 2.0036. The modulation amplitude was suited at 4 Gauss while the microwave frequency was determined as 9.775 GHz. Elemental microanalysis was performed at the Micro-analytical Center of Cairo University using Elementer Vario EL III. The copper content was determined by complexometry [16]. TG/DTA analysis was performed in a dinitrogen atmosphere (20 mL min^{-1}) in a platinum crucible with a heating rate of $10 \text{ }^\circ\text{C min}^{-1}$ using a Shimadzu DTG-60H simultaneous DTG/TG apparatus. A digital Jenway 4330 conductivity/pH meter with a cell constant of 1.02 was used for the pH and molar conductance measurements.

Computational details

Geometry optimizations of complexes **1** and **2** were carried out without symmetry restrictions in the doublet state, whereas a singlet state was assigned to binuclear complex **3**. All calculations were carried out using Gaussian03 [17] in both the gas phase and a DMSO solvent using the polarizable continuum model (PCM) via the B3LYP functional and a LANL2DZ basis set [9,14,15]. The studied complexes were characterized as local minima through harmonic frequency analysis and their vibrational spectra were analyzed using the Gaussview software for absence of imaginary modes [18]. Electronic excitations were obtained by TDDFT [19]. Natural bond orbital analysis [20], molecular electrostatic potential calculations and the analysis of frontier molecular orbitals were performed at the same level of theory and ionization energies, electron affinities, electronegativity, softness, hardness and electrophilicity index were calculated [4,9,10].

Antibacterial activity

The antibacterial activity of compounds was tested on *Staphylococcus aureus* as a Gram-positive bacterium, and *Escherichia coli* as a Gram-negative bacterium according to a modified Kirby-Bauer disc diffusion method under standard conditions using Mueller-Hinton agar medium (tested for composition and pH), as previously reported [15]. The LC₅₀ (μmol/mL), the concentration that inhibit 50% of bacterial growth with respect to the control, was determined.

Results and discussion

IR assignments

The coordination behavior of **H₂L** to Cu^{II} centre was carefully estimated with the aid of the calculated normal modes. IR spectrum of **H₂L** shows a band at 3377 cm⁻¹ assigned to ν(NH), while the ν(OH) mode could not be experimentally allocated due to C=N_{Azo}···O—H interaction [21]. The broad band(s) at 3426 cm⁻¹ (**1**), 3409 cm⁻¹ (**2**) as well as 3559 and 3388 cm⁻¹ in **3** is assigned to ν(OH₂). Complex **1** exhibits a band at 1546 cm⁻¹ assigned to δ_s(-OH₂). The disappearance of ν(NH) mode in **1** and **3** revealed the ionization of SO₂NH upon complex formation. The ν_{ss}(SO₂) is observed at 1150, 1141 and 1145 cm⁻¹ in **H₂L**, **1** and **2** excluding the coordination via SO₂ group [11]. For **3**, this vibration mode is overlapped with the numerous bands of NO₃ group. A shift of ν(S—N) band to high wave numbers, 978 (**1**) and 986 cm⁻¹ (**3**), is due to ionization of SO₂NH and a concomitant enforcement of the S—N distance [9]. As expected [21], the ν(C=N_{Azo}) of **H₂L** is overlapped with ν(C=C) modes due to intra H-bond. This mode appears at 1605 cm⁻¹ in binuclear **3**, and is still overlapped in **1** and **2**.

Complex **1** has two new bands at 1385 and 1288 cm⁻¹ due to NO₃⁻ (ν₃) mode with a separation of 97 cm⁻¹ supporting a monodentate nature [22,23], whereas the weak band at 785 cm⁻¹ is assigned to the in-plane bending mode (ν₄). The involvement of NO₃⁻ in the primary coordination sphere is confirmed by existence of a weak band near 1000 cm⁻¹ (ν₁) [24]. For **2**, the medium band at 1381 cm⁻¹ is assigned to ν₃(NO₃⁻). Other bands, characterize NO₃⁻, are overlapped with numerous bands of the coordinated **H₂L**. Complex **3** shows two new bands at 1375 and 1315 cm⁻¹ assigned to monodentate NO₃⁻ (ν₃). Besides, the bands at 943 cm⁻¹ (ν₁), 872 cm⁻¹ (ν₂), 750 and 743 cm⁻¹ (ν₄) are assigned to NO₃⁻ groups. The new band at 587 (**2**) and 598 cm⁻¹ (**3**) is due to ν(Cu—O) of phenolic group, whereas the bands at 480 and 425 cm⁻¹ in **3** are accounted for ν(Cu—O) of nitrate and water molecules, respectively [25].

TG/DTA analysis

The thermal decomposition of **1** was accompanied by loss of 4H₂O, 12.48% (calcd. 12.43%), via two overlapping endothermic peaks at 55 and 213 °C. The 2nd main stage is multipart with three peaks at 320, 351 and 400 °C, assigned to removal of HL and NO₂, leaving CuO as a residue, with an amount of 13.28% (calcd. 13.73%). For **2**, the 1st and 2nd endothermic stages are assigned to desorption of 3 H₂O (observed mass loss 9.69%, calcd. 9.62%). The 3rd and 4th events are thought to be due to loss of HL and NO₃, giving Cu/CuO as deposit at 1000 °C with a remaining mass of 12.60% (calcd. 12.74%). The TG/DTA curves of **3** shows three peaks at 59, 199, and 257 °C assigned to removal of 6 H₂O amounts to 14.65%. The mass loss of the three additional endothermic peaks at 450, 650, and 1004 °C is as expected for the removal of L + 2NO₂, leaving CuO with a mass 21.51% (calcd. 21.75%).

Geometry optimization and NBO analysis

The copper atom in complex **1** (Fig. 2a) adopts a distorted square pyramidal geometry. The basal plane of the pyramid is defined by two nitrogen atoms, the sulfonamidic [Cu—N13 = 2.032 Å] and pyrimidic [Cu—N21 = 2.081 Å] ones. These are in a trans position (<N13CuO31, 91.8°) relative to a water molecule [Cu—O33 = 1.987 Å] and oxygen-coordinated nitrate [Cu—O36 = 2.023 Å]. A second water molecule [Cu—O39 = 2.180 Å] occupies the axial position. This geometry appears distorted as can be seen from the spread in the bond distances (1.987–2.180 Å) and angles (65.1–106.4°). Cu—O36(NO₃) bond distance is in agreement with the other copper complexes, 2.029 Å [26], coordinated by a terminal nitrate. The other oxygen O31 of the nitrate group is close to Cu atom by 2.964 Å. If this distance is short enough to be considered as Cu—O interaction, the coordination polyhedron around Cu can be considered as a highly distorted octahedral.

On the other hand, the basal plane around the copper atom in complex **2** (Fig. 2b) is formed by three oxygen atoms (O44, O46 and O50) with bond distances of 1.920, 2.042, and 1.996 Å from two water molecules in a *cis* arrangement and the deprotonated phenolate group as well as the nitrogen atom of the azomethine N [Cu—N11 = 1.990 Å]. The axial position is occupied by a water molecule (O47). The elongation of the axial bond distance is due to the Jahn–Teller effect, which is typical for a 3d⁹ electron configuration in a square–pyramidal coordination environment [11]. The O44—Cu—O46 and N11—Cu—O50 angles somewhat deviate from linearity and are at 165.4° and 174.5°. This is indicative of an irregular structure. For pentacoordinated complexes, the angular structural index parameter τ ($\tau = (\alpha - \beta)/60^\circ$; α and β are the two largest angles) was introduced [27], with $\tau = 0$ for a perfect square–pyramidal and $\tau = 1$ for a perfect trigonal–bipyramidal geometry. In the case of complexes **1** and **2**, τ values of 0.25 and 0.15 were determined, respectively, which shows a slightly deviation from a square–pyramidal coordination environment. As shown in Fig. 2c, each of the two independent copper centers (Cu33 and Cu51) in the binuclear complex **3** are also in five-coordinated square pyramidal geometry. Comparison between complexes **2** and **3** (Table S1) showed the elongation of N11Cu51 and O52Cu51 bond by 0.026 and 0.054 Å upon introduction of another metal ion. Similar, the N13Cu and O39Cu in **1** are short by ≈0.03 Å with respect to complex **3**.

NBO [20] and second order perturbation theory analysis of Fock Matrix provide details about the type of hybridization, nature of bonding and strength of the interactions between metal ion and donor sites [28]. The electronic arrangement, 3d electrons distribution and natural atomic charge of Cu^{II} in the reported complexes are presented in Table 1. For example, the atomic charge upon Cu^{II} (+1.067e) in **1** is higher than that of **2** (+1.056e). This may be

Table 1
Electronic configuration, 3d populations and charge of Cu atom in the studied complexes.

Complex	Electronic arrangement	d_{xy}	d_{xz}	d_{yz}	$d_{x^2-y^2}$	d_{z^2}	Charge on Cu atom
1	[core]4s ^{0.26} 3d ^{9.29} 4p ^{0.38} 5p ^{0.01}	1.703	1.970	1.955	1.669	1.989	1.067e
2	[core]4s ^{0.27} 3d ^{9.32} 4p ^{0.35}	1.917	1.994	1.971	1.971	1.979	1.056e
3	[core]4s ^{0.24} 3d ^{9.49} 4p ^{0.24} 5p ^{0.13} (Cu33)	1.981	1.959	1.959	1.602	1.984	0.904e
	[core]4s ^{0.24} 3d ^{9.50} 4p ^{0.35} (Cu51)	1.552	1.985	1.991	1.991	1.978	0.901e

[Core] = 18 electrons.

attributed the high electronegativity of phenolate O with respect to the sulfonamidic N. The strength of interaction between Cu^{II} and ligand active sites in the reported complexes has been assigned by second order interaction (E^2). The E^2 values of **1** are 1.02 and 0.85 kcal mol⁻¹ for LP(1)N13 → RY*(5)Cu and LP(1)N21 → RY*(4)-Cu, respectively. For **2**, the E^2 values are 1.45 and 0.83 kcal mol⁻¹ for LP(1)N11 → RY*(1)Cu and LP(2)O44 → RY*(1)Cu. By comparison, Cu^{II} will preferably bind to sulfonamidic N13 than phenolate O44 atom that may be due to the high negatively charge of N13 (-0.9098e) comparing with that of O44 (-0.7360e). Similar, the interaction of Cu^{II} with azomethine N11 is stronger than the pyrimidic N21. This is due to the sharing of N21 in resonating structures within the pyrimidine moiety. The binding energy [9] of **1** is larger than **2** by 866 cal mol⁻¹, but lower than **3** by 1483.746 cal mol⁻¹ revealing the higher stability of the binuclear complex (Table S2). Hence, the stronger the binding capability is, the more stable the complex will be.

Electronic structure

Sodium sulfamethazine shows a single absorption band at 274 nm in DMF [10]. Likewise, **H₂L** exhibits one broad band (in DMF) at 276 nm and a shoulder at 340 nm assigned to $\pi-\pi^*$ transition of C=N_{Azo}. The pH dependency of the absorption spectrum of sodium sulfamethazine (NaSMZ) and **H₂L** was investigated in the pH = 2–12 range (Fig. S1). Two deprotonation steps with pKa values of 2.70 and 8.45 are reported for NaSMZ in aqueous medium and assigned to the deprotonation of -NH₃⁺ and ionization of -SO₂-NH, respectively. In contrast, a three-step process with pKa values of 2.83, 7.46, and 9.04 was determined for **H₂L** in 20% ethanol/water. These are assigned to the deprotonation of -NH₃⁺, phenolic OH and -SO₂NH, respectively. Copper complex **1**, with the metal center bound to the sulfonamide part of the ligand, only shows one intense absorption centered just below 290 nm, with a broad tail extending from about 340 to 490 nm. Compounds **2** and **3**, in which the Schiff-base part is involved in binding of the transition metal moiety, the main peak also appears at around 280 nm but the long-wavelength tail is more pronounced (Fig. S2). The main band near 280 nm is attributed to intra-ligand $\pi-\pi^*$ transitions. For complexes **2** and **3**, the $\pi-\pi^*$ transition of C=N_{Azo} is shifted to longer wavelengths and appears at 355 and 357 nm, respec-

tively. This supports the involvement of the C=N_{Azo} group in chelation. In addition, the shoulders observed at 454, 464, and 413 nm in **1**, **2**, and **3** are due to LMCT transitions involving the phenolate, and pyrimidine moieties [29].

This assignment is supported by TDDFT studies. For compound **1**, four main absorption bands at 816, 525, 411, and 397 nm with oscillator strengths of 0.0034, 0.0527, 0.0064 and 0.0072 were calculated (Table 2). The broad calculated band at 816 nm is arising from transitions of β -spin HOMO-1/HOMO-23 to β -spin LUMO. As shown in Fig. 3, the LUMO orbital with β -spin is mainly of Cu $d_{x^2-y^2}$ character with contributions from π -bonding of the azomethine/aniline/salicylaldehyde moiety. The HOMO-23 orbital is of mixed Cu d_{z^2} , NO₃, H₂O and pyrimidine contributions. β -spin HOMO-1 orbital is contained upon aniline residue. Hence, the weak absorption band at 816 nm, which is close to $d_{z^2} \rightarrow d_{x^2-y^2}$ transition energy characterized to square pyramidal geometry, is mainly $\pi(\text{An}) \rightarrow d_{x^2-y^2}$ LMCT in nature. This is due to high lying occupied π -bonding MO of the aromatic moieties. The excitation energy at 525 nm (2.36 eV) is contributed mainly from HOMO-2(β) → LUMO(β) (70%). This transition is predominantly $\pi/d \rightarrow d_{x^2-y^2}$ in nature. The highest energy transitions at 411 and 397 nm assigned to HOMO-3(β)/HOMO-5(β) to LUMO(β), respectively, bear some sort of LMCT. For **2** complex, the lowest energy electronic transition at 529 nm (2.34 eV, $f = 0.0026$) characterizes HOMO-30(β) → LUMO(β) (21%), while that at 398 nm is arises from a transition of α -spin HOMO-1 to α -spin LUMO (34%).

EPR and magnetic measurements

Room temperature EPR spectra on powdered samples were recorded at X-band frequency (Fig. S3). Intense signals are observed which do not show any noticeable ^{63/65}Cu ($I = 3/2$) hyperfine splitting. The average g -values slightly decrease in the order **2** > **1** > **3**. Five-coordinated Cu^{II} complexes may be present in either square pyramidal or trigonal bipyramidal geometry. In square-pyramidal complexes, $g_{\parallel} > g_{\perp}$ and the value of the hyperfine splitting (A_{\parallel} is between 120 and 150 × 10⁻⁴ cm⁻¹, whereas the trigonal-bipyramidal complexes are characterized by $g_{\perp} > g_{\parallel}$ and $A_{\parallel} = 60 - 100 \times 10^{-4}$ cm⁻¹ [30]. Hence, according to Table 3, the reported compounds established a distorted square-pyramidal geometry. The geometric parameter G , which is a measure of

Table 2
Computed excitation energies (eV), electronic transition configurations and oscillator strengths (f) of the studied complexes (selected, $f > 0.001$).

Exp.	λ (nm)	E (eV)	f	Major contributions	Character	
Complex 1	816	1.5191	0.0034	HOMO-1(β) → LUMO(β) (27%) HOMO-23(β) → LUMO(β) (11%)	$\pi(\text{An}) \rightarrow d/\pi^*(\text{Azom}/\text{An}/\text{Saly})$ $d/\pi(\text{NO}_3)/(\text{H}_2\text{O})/\pi(\text{Py}) \rightarrow d/\pi^*(\text{Azom}/\text{An}/\text{Saly})$	
	736	1.6823	0.0022	HOMO-16(β) → LUMO(β) (34%)	$\pi(\text{NO}_3)/(\text{SO}_2)/\pi(\text{An}/\text{Saly}) \rightarrow d/\pi^*(\text{Azom}/\text{An}/\text{Saly})$	
	454	525	2.3609	0.0527	HOMO-2(β) → LUMO(β) (70%)	$d/\pi(\text{Py}) \rightarrow d/\pi^*(\text{Azom}/\text{An}/\text{Saly})$
	357	411	3.0166	0.0064	HOMO-3(β) → LUMO(β) (40%)	$\pi(\text{An}/\text{Saly}) \rightarrow d/\pi^*(\text{Azom}/\text{An}/\text{Saly})$
		397	3.1221	0.0072	HOMO-5(β) → LUMO(β) (38%)	$\pi(\text{Py})/(\text{SN})/\pi(\text{An}/\text{Saly}) \rightarrow d/\pi^*(\text{Azom}/\text{An}/\text{Saly})$
	Complex 2	529	2.3433	0.0026	HOMO-30(β) → LUMO(β) (21%)	$\pi(\text{SO}_2)/\pi(\text{An})/\pi(\text{Azom}) \rightarrow d/\pi^*(\text{Azom}/\text{An}/\text{Saly})$
464		398	3.1117	0.0519	HOMO-1(α) → LUMO(α) (34%)	$d/\pi(\text{An}) \rightarrow d/\pi^*(\text{NO}_3)/\pi^*(\text{An})$
355		360	3.4398	0.0069	HOMO-11(β) → LUMO(β) (20%)	$\pi(\text{SO}_2) \rightarrow d/\pi^*(\text{Azom}/\text{An}/\text{Saly})$
		345	3.5856	0.0346	HOMO-12(β) → LUMO(β) (29%)	$\pi(\text{Azom}/\text{An}/\text{Saly}) \rightarrow d/\pi^*(\text{Azom}/\text{An}/\text{Saly})$

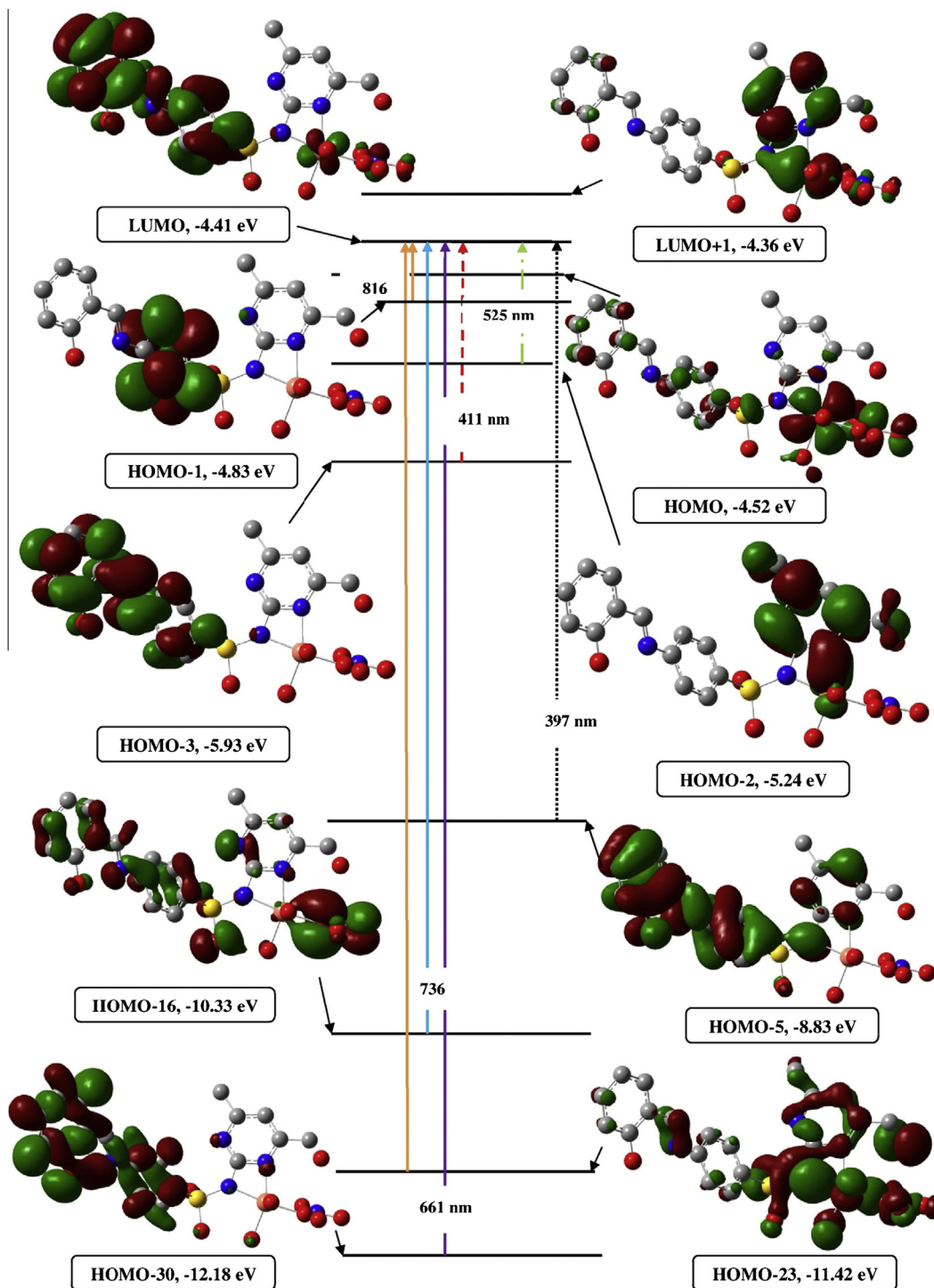


Fig. 3. TDDFT-calculated electronic transitions in complex 1.

exchange of interaction between Cu centers in a powdered sample, has been calculated as follows: $G = (g_{\parallel} - 2.0023)/(g_{\perp} - 2.0023)$ [31] for axial spectra and for rhombic spectra $G = (g_3 - 2.0023)/(g_1 - 2.0023)$ and $g_{\perp} = (g_1 + g_2)/2$. According to Hathaway and Billing [32] if $G > 4$, the exchange interaction is negligible and if $G < 4$, indicates presence of some sort of interaction. The G value decreases in the order $2 > 1 > 3$, indicating weak interaction among **1** and **3** molecules.

The g -tensor was calculated using unrestricted DFT functional of MPW1PW91, B3PW91, PBEPBE and B3LYP combined with

DGDZVP basis set using gauge including atomic orbitals (GIAO) [33]. In the present study, the spin-restricted DFT method developed by Rinkevicius et al. [34] was used. In this formalism, the g tensor is calculated as a correction Δg to the free electron value g_e (2.0023).

$$g = \Delta g_{RMC} + \Delta g_{GC(1e)} + \Delta g_{OZ/50} + g_e$$

Δg describes the influence of the local electronic environment in the molecule on the unpaired electron (s) compared to the free electron. The g tensor shift contains two minor contributions, namely

Table 3
Experimental and theoretical EPR parameters of the studied **1–3** complexes.

Complex	Exp.			Theoretical							
	g_{\parallel}	g_{\perp}	G	B3LYP		B3PW91		MPW1PW91		PBEPBE	
				g_{\parallel}	g_{\perp}	g_{\parallel}	g_{\perp}	g_{\parallel}	g_{\perp}	g_{\parallel}	g_{\perp}
1	2.408	2.108	3.86	2.283	2.149	2.229	2.118	2.314	2.165	2.158	2.080
2	2.415	2.108	4.07	2.262	2.088	2.2155	2.071	2.290	2.098	2.154	2.050
3	2.407	2.108	3.84								

the mass-velocity (Δg_{RMC}), and the one-electron gauge ($\Delta g_{GC(1e)}$) corrections to the electronic Zeeman effect, along with the dominating spin-orbit (SO) contribution, $\Delta g_{OZ/SO}$. The theoretical EPR studies of the mononuclear complexes showed axial spectra, with a unique axis that differs from the other two ($g_x = g_y \neq g_z$). The g factor along the unique axis is said to be parallel, $g_z = g_{\parallel}$ while the remaining two axes are perpendicular to it, i.e. $g_{\perp} = (g_x + g_y)/2$. As shown in Table 3, calculated g -tensor values showed best agreement with experimental values when carried out using the MPW1PW91 functional, while PBEPBE is less accurate.

The observed effective magnetic moment (μ_{eff}) values, corrected for diamagnetic and temperature-independent paramagnetic contributions, were found to be 1.73 and $1.74\mu_B$ (296 K) for the mononuclear complexes **1** and **2**, respectively, and $3.21\mu_B$ (per Cu_2) for **3**. These values are close to the spin-only values expected for non-interacting Cu^{II} ions ($S = 1/2$, $t_{2g}^6 e_g^3$), $\mu_{\text{eff}} = 1.73\mu_B$, and in the acceptable range for copper complexes ($1.60\text{--}1.80\mu_B$). This indicates the presence of monomeric species without any interaction between the Cu^{II} ions from neighboring molecules [35] and a lack of intramolecular magnetic coupling between the two copper centers in dinuclear compound **3**.

Antibacterial activity

The antibacterial activity of organic ligand **H₂L** as well as its copper(II) complexes **1–3** were tested on against *S. aureus* as a Gram-positive and *E. coli* as a Gram-negative microorganism and compared to tetracycline used as a standard. Preliminary screening was carried out at 20 mg/mL. As expected [36], **H₂L**

is significantly more toxic against Gram-positive than Gram-negative bacteria, which is due to the different cell wall structure of the tested microorganisms, while the reference compounds sodium sulfamethazine and tetracycline show almost equal activity against both strains tested. Although **H₂L** shows quite some activity against *S. aureus*, it is less toxic than the two established drugs (Fig. 4). These differences might be due to the absence of a primary amino group in the ligand **H₂L** due to the Schiff base formation with salicylic aldehyde and the non-planarity of the two phenyl rings ($\text{C5-C6-N11-C32} = 37.4^\circ$) [37]. As known [9], the active species of sulfonamides is the ionic form, so the proton-ligand formation constant of $-\text{SO}_2\text{NH}$ will be the third variable contributed to the lower antibacterial activity of the ligand **H₂L** comparing with sodium sulfamethazine.

Coordination to a copper(II) center, regardless of the binding site and Cu:L stoichiometry, leads to a significant decrease in antibacterial activity compared to the free ligand as well as reference drugs in the case of *S. aureus* and almost completely abolishes it for the dinuclear compound **3** while relative differences between **1** and **2** are small. Interestingly, the trend is reversed for *E. coli*. While both **H₂L** and dicopper complex **3** are inactive on this Gram-negative microorganism, the antibacterial activity of **2** and **3** almost reaches that found in the Gram-positive case, although it still remains much lower than that of sodium sulfamethazine and tetracycline. In absolute terms, identical LC_{50} values of $0.27\mu\text{mol/mL}$ were determined for **1** and **2** against *S. aureus*. This is about twofold lower than for the free ligand **H₂L** ($0.12\mu\text{mol/mL}$) but higher than for the dinuclear complex **3** ($0.62\mu\text{mol/mL}$).

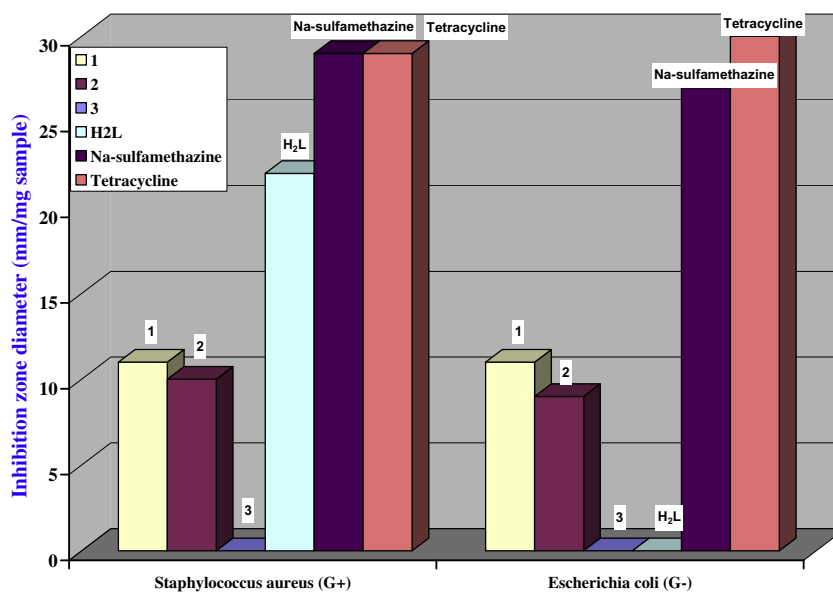


Fig. 4. Antibacterial activity of ligand **H₂L** and copper complexes **1–3** as well as sodium sulfamethazine and tetracycline against *S. aureus* as a Gram-positive, and *E. coli* as a Gram-negative microorganism. All experiments were carried out in triplicate and the mean results are given. DMSO was used as a control and its inhibition zone was subtracted from the others in each case.

Structure–activity relationship (SAR)

The ultimate aim of SAR studies [38] is to correlate the biological activity of a series of compounds with some appropriate quantum chemical descriptors based on DFT (Table S2). Different descriptors such as E_{HOMO} , E_{LUMO} , energy gap, ionization energy, electron affinity, dipole moment, hardness (η), softness (S), electrophilicity index (ω), polarizability (α), and electronegativity (χ) were tested for SAR analysis. Fig. 5 shows some representative plots of the correlations made between the experimental LC_{50} and quantum chemical parameters/descriptors.

Frontier molecular orbitals [39], can determine the way in which the molecule interacts with other species. E_{HOMO} is associated with the electron donating ability, while E_{LUMO} indicates the ability of the molecule to accept electrons. Smaller E_{LUMO} means minor resistance to accept electrons. Herein, a good correlation ($R^2 = 0.8895$) is found between LC_{50} and E_{LUMO} , and the toxicity of the studied compound increases as the energy of LUMO increases. HOMO–LUMO gap (ΔE) is an important stability index that can decide whether the molecule is hard or soft. Soft molecule is more polarizable than the hard one. For the active compounds

studied in this work, high ΔE value (hard) of H_2L correlates well ($R^2 = 0.9873$) with a high activity. Thus, less active complexes are more stable than the active H_2L .

Hydrophobicity descriptor (usually expressed as $\text{Log}P$) represents the ability of molecule to enter the cell membrane and contact with the interacting sites. Hydrophobicity is related to the free energy change associated with the desolvation of a compound as it moves from an aqueous phase to the biological part. Fat-soluble drugs are easily absorbed, whereas water-soluble one is difficult to absorb. Dipole moment (μ in Debye) was used to qualitatively analyze the trend in the hydrophobic values ($\text{Log}P$). A very significant dipole moment may polarize the molecule in such a way that it produces a required potential at several atomic centers necessary for binding and activity. Hence, the smallest dipole moment value of H_2L should be a considerable factor for its highest antibacterial activity. This behavior happens together with the lowest polarizability (α) of the free ligand H_2L . Alternatively, electrophilicity index (ω) is a descriptor that accounts for the positively charge property in a molecule that also has high capability to scavenge electrons or superoxide anions. This property is correlated well with LC_{50} values of the studied compounds with R^2 of 0.9878

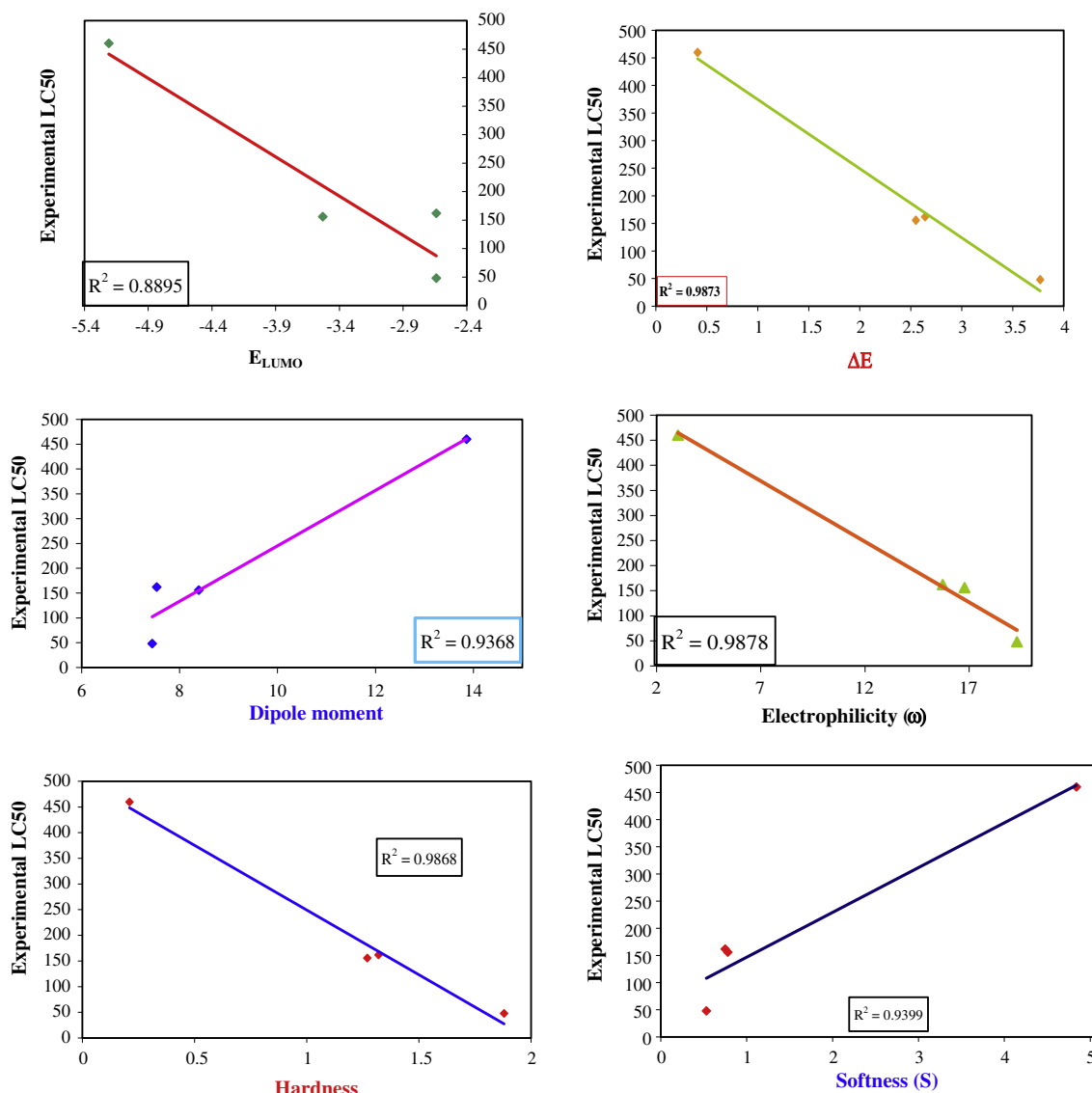


Fig. 5. Correlations between experimental LC_{50} and different quantum chemical parameters for H_2L and its copper complexes.

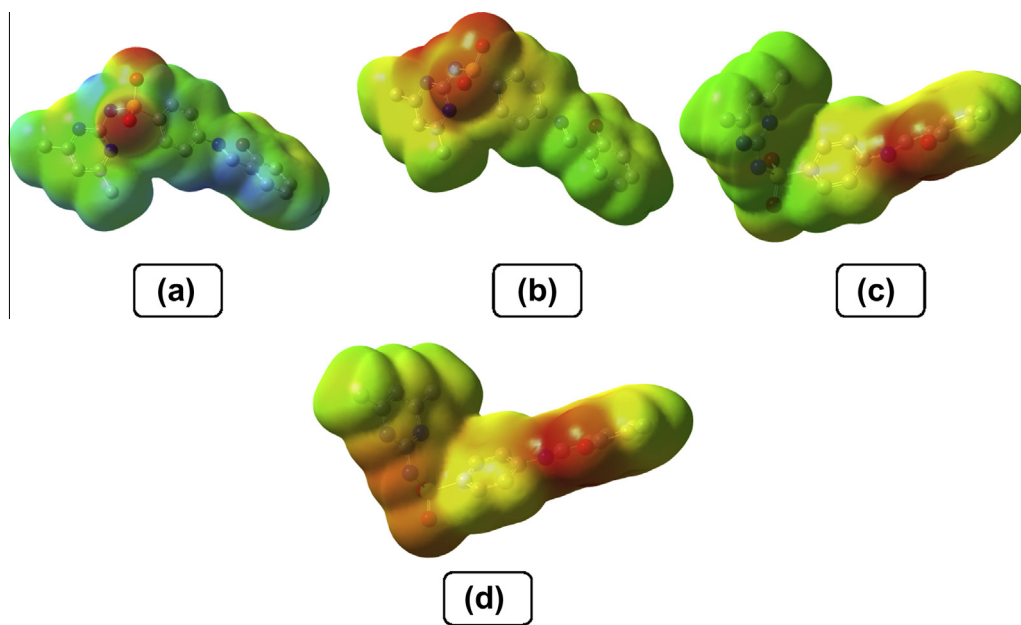


Fig. 6. Molecular electrostatic potential for (a) H_2L , (b) HL^- ($-\text{NH}$), (c) HL^- ($-\text{OH}$), and (d) L^{2-} . The electron density isosurface is 0.004 a.u.

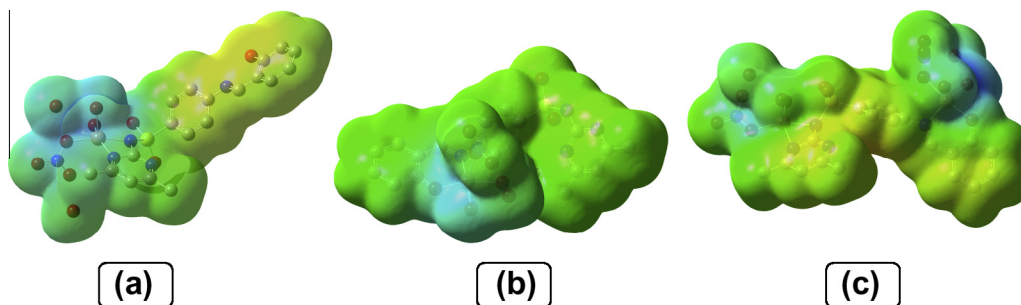


Fig. 7. Molecular electrostatic potential of complexes (a) 1, (b) 2, and (c) 3. The electron density isosurface is 0.004 a.u.

indicated that a high value of ω is observed for compound H_2L that displays highest activity among the studied compounds.

Molecular electrostatic potential (MEP) map is a very useful descriptor in understanding sites for electrophilic attack, nucleophilic reactions and hydrogen bonding interactions [9,10]. Different values of the electrostatic potential are represented by different colors: red represents regions of most electro negative electrostatic potential, blue represents regions of most positive electrostatic potential and green represents regions of zero potential. Potential increases in the following order: red < orange < yellow < green < blue. As shown in Fig. 6a, a weak negatively MEP value ($-0.060e$) is localized upon phenolic O in organic ligand H_2L , and strong negative regions ($-0.090e$) are mainly contained on SO_2 group. Both phenolic O and SO_2 groups can act as centers for several H bond with the neighboring molecules. In contrast, maximum positive regions are found over hydrogen atoms of $\text{SO}_2\text{-NH}$ ($+0.067e$) and CH=N ($+0.077e$) groups. For HL^- (Fig. 6b), red¹ regions are extended and become more strongly to cover N13, N21 and SO_2 after ionization of $-\text{SO}_2\text{NH}$. This confirms that the ionic form of H_2L is the truly antimicrobial species as previously mentioned. The ionic sulfonamide site may constitute the preferable location for binding with metal atoms such as Na^+ or K^+ , the interaction of

which will result in increased binding capacity leading to enhanced activity. Likewise, if HL^- is formed through the ionization of OH group, the surface map of phenolic O will be increased to attain $-0.282e$ that may act as another source for the biological activity (Fig. 6c). Thus, it can be concluded that the pKa values of SO_2NH , OH groups and the negative charge upon SO_2 are contributed to the bacteriostatic activity of the investigated compounds. This is confirmed by the increase in the surface map values of N13, N21, O49 and SO_2 after ionization of both OH and NH protons to form L^{2-} (Fig. 6d) comparing with HL^- .

For copper(II) complexes, a strong positive region is located over the metal centre at the base of the pyramidal with a small contribution on the hydrogen atoms of the coordinated H_2O (Fig. 7). As shown in Fig. 7a, some aromatic areas and phenolic O in **1** are tinted with yellow color (slightly negative surface). This site may be responsible for the antibacterial activity of compound **1**. Similar, a yellow region is found upon $-\text{SO}_2\text{NH}$ group in **2**. Alternatively, blue regions cover up copper centers in the binuclear compound **3** (Fig. 7c), whereas negative regions are found on aniline moiety and the non-coordinated pyrimidine N22 that would be ideal for docking and interaction with cell wall structure of the tested microorganisms. Thus, the toxicity of the complexes can be related to the strength of surface map value and regions of highest negative potential may be suitable for H-bonding and/or complex formation.

¹ For interpretation of color in Fig. 6, the reader is referred to the web version of this article.

4. Conclusion

Three new mono- and dinuclear copper(II) complexes of a Schiff-base functionalized sulfamethazine antibacterial drug were prepared, characterized, and tested for biological activity against *S. aureus* and *E. coli*. Coordination to a copper(II) center, regardless of the binding site and Cu:L stoichiometry, resulted in a significant decrease of antibacterial activity compared to the free ligand as well as the reference drugs tested. While the binuclear compound was completely inactive, the two mononuclear compounds, only varying in the binding pocket occupied by the copper moiety, showed relatively low but comparable activity against both Gram-positive and negative microorganisms. SAR studies suggested that E_{LUMO} , energy gap, dipole moment, polarizability and electrophilicity index values were the most significant descriptors for correlating the molecular structures of the studied compounds and their respective antibacterial activity.

Acknowledgments

I thank Prof. Dr. U. Schatzschneider, Julius-Maximilians-Universität Würzburg, Germany for the proof-reading of this manuscript. I would like to extend our grateful thanks to Prof. Dr. N.T. Abdel-Ghani, Chemistry Department, Faculty of Science, Cairo University for continuous encouragement throughout the present work.

Appendix A. Supplementary material

Supplementary data associated with this article can be found, in the online version, at <http://dx.doi.org/10.1016/j.saa.2013.12.066>.

References

- [1] S. Roland, R. Ferone, R.J. Harvey, V.L. Styles, R.W. Morrison, *J. Biol. Chem.* 254 (1979) 10337–10345.
- [2] M.E. Wolff (Ed.), *Burger's Medicinal Chemistry and Drug Discovery*, fifth ed., vol. 2, Wiley, Laguna Beach, 1996, pp. 528–576.
- [3] (a) I.P. Kaur, M. Singh, M. Kanwar, *Int. J. Pharm.* 199 (2000) 119–127; (b) G.L. Plosker, D. Tavish, *Drugs* 47 (1994) 622–651.
- [4] A.M. Mansour, N.T. Abdel-Ghani, *J. Mol. Struct.* 1040 (2013) 226–237 (and the references herein).
- [5] (a) J.B. Tommasino, F.N.R. Renaud, D. Luneau, G. Pilet, *Polyhedron* 30 (2011) 1663–1670; (b) L. Gutiérrez, G. Alzuet, J. Borrás, A. Castiñeiras, A. Rodríguez-Fortea, E. Ruiz, *Inorg. Chem.* 40 (2001) 3089–3096; (c) M. Gaber, H.E. Mabrouk, Y.M. Shaibi, A.A. Ba-Issa, *Thermochem. Acta* 207 (1992) 239–244.
- [6] (a) N.C. Baenziger, S.L. Modak, C.L. Fox, *Acta Crystallogr.* C39 (1983) 1620–1623; (b) C.J. Brown, D.S. Cook, L. Sengier, *Acta Crystallogr.* C41 (1985) 718–720.
- [7] (a) N.C. Baenziger, A.W. Struss, *Inorg. Chem.* 15 (1976) 1807–1809; (b) D.S. Cook, M.F. Turner, *J. Chem. Soc. Perkin Trans.* 2 (1975) 1021–1025.
- [8] F. de Zayas-Blanco, M.S. García-Falcón, J. Simal-Gándara, *Food. Contr.* 15 (2004) 375–378.
- [9] A.M. Mansour, *Inorg. Chim. Acta* 394 (2013) 436–445.
- [10] A.M. Mansour, *J. Mol. Struct.* 1035 (2013) 114–123.
- [11] A.M. Mansour, *J. Coord. Chem.* 66 (7) (2013) 1118–1128.
- [12] Z.H. Chohan, M.N. Tahir, H.A. Shada, I.U. Khan, *Acta Cryst.* E64 (2008) o648.
- [13] H.A. Shada, M.N. Tahir, Z.H. Chohan, *Acta Cryst.* E65 (2009) o98–o99.
- [14] N.T. Abdel-Ghani, A.M. Mansour, *Inorg. Chim. Acta* 373 (2011) 249–258.
- [15] N.T. Abdel-Ghani, A.M. Mansour, *Eur. J. Med. Chem.* 47 (2012) 399–411.
- [16] A. Skoog, D.M. West, *Fundamentals of Analytical Chemistry*, Thomson, Brooks, Cole, New York, 2004.
- [17] M.J. Frisch, G.W. Trucks, H.B. Schlegel, G.E. Scuseria, M.A. Robb, J.R. Cheeseman, V.G. Zakrzewski, J.A. Montgomery, R.E. Stratmann, J.C. Burant, S. Dapprich, J.M. Millam, A.D. Daniels, K.N. Kudin, M.C. Strain, O. Farkas, J. Tomasi, V. Barone, M. Cossi, R. Cammi, B. Mennucci, C. Pomelli, C. Adamo, S. Clifford, J. Ochterski, G.A. Petersson, P.Y. Ayala, Q. Cui, K. Morokuma, D.K. Malick, A.D. Rabuck, K. Raghavachari, J.B. Foresman, J. Cioslowski, J.V. Ortiz, A.G. Baboul, B.B. Stefanov, G. Liu, A. Liashenko, P. Piskorz, I. Komaromi, R. Gomperts, R.L. Martin, D.J. Fox, T. Keith, M.A. Al-Laham, C.Y. Peng, A. Nanayakkara, C. Gonzalez, M. Challacombe, P.M.W. Gill, B.G. Johnson, W. Chen, M.W. Wong, J.L. Andres, M. Head-Gordon, E.S. Replogle, J.A. Pople, *GAUSSIAN 03 (Revision A.9)*, Gaussian Inc., Pittsburgh, 2003.
- [18] A. Frisch, A.B. Nielson, A.J. Holder, *GAUSSVIEW User Manual*, Gaussian Inc., Pittsburgh, PA, 2000.
- [19] N.T. Abdel-Ghani, A.M. Mansour, *J. Coord. Chem.* 65 (5) (2012) 763–779.
- [20] F. Weinhold, J.E. Carpenter, *The Structure of Small Molecules and Ions*, Plenum, New York, 1988 (pp. 227).
- [21] N.T. Abdel-Ghani, A.M. Mansour, *Spectrochim. Acta* 81 (2011) 754–763.
- [22] M.A. Maldonado-Rogado, E. Viñuelas-Zahinos, F. Luna-Giles, A. Bernalte-García, *Polyhedron* 26 (2007) 1173–1181.
- [23] N.F. Curtis, Y.M. Curtis, *Inorg. Chem.* 4 (1965) 804–809.
- [24] B.M. Gatehouse, S.E. Livingstone, R.S. Nyholm, *J. Chem. Soc.* (1957) 4222–4225.
- [25] K. Nakamoto, *Infrared and Raman Spectra of Inorganic and Coordination Compounds, Part B: Applications in Coordination, Organometallic, and Bioinorganic Chemistry*, sixth ed., John Wiley & Sons Inc., New Jersey, 2009.
- [26] J. Pons, A. Chadghan, J. Casabo, A. Alvarez-Larena, J. Francesc Piniella, J. Ros, *Polyhedron* 20 (2001) 2531–2536.
- [27] A.W. Addison, T.N. Rao, J. Reedijk, J.V. Rijn, G.C. Verschoor, *J. Chem. Soc. Dalton Trans.* (1984) 1349–1356.
- [28] N.T. Abdel-Ghani, A.M. Mansour, *Spectrochim. Acta* 81 (2011) 529–543.
- [29] M. Mijanuddin, A. Ray, P. Chandra-Mondal, J. Marek, M. Ali, *J. Mol. Struct.* 826 (2007) 17–23.
- [30] B.J. Hathaway, G. Wilkinson, R.G. Gillard, J.A. McCleverty (Eds.), *Comprehensive Coordination Chemistry*, vol. 5, Pergamon Press, Oxford, 1987, p. 533.
- [31] R.J. Rudley, B.J. Hathaway, *J. Chem. Soc.* (1970) 1725–1728.
- [32] B.J. Hathaway, D.E. Billing, *Coord. Chem. Rev.* 5 (1970) 143–207.
- [33] N.T. Abdel-Ghani, A.M. Mansour, *Spectrochim. Acta* 91 (2012) 272–284.
- [34] Z. Rinkevicius, L. Telyatnyk, P. Salek, O. Vahtras, H. Ågren, *J. Chem. Phys.* 119 (2003) 34–46.
- [35] G. Albertin, E. Bordignon, A.A. Orío, *Inorg. Chem.* 14 (1975) 1411–1413.
- [36] A.L. Koch, *Clin. Microbiol. Rev.* 16 (2003) 673–687.
- [37] (a) P.H. Bell, R.O. Roblin, *J. Am. Chem. Soc.* 64 (1942) 2905–2917; (b) J.K. Seydel, *J. Pharm. Sci.* 57 (1968) 2905–2917.
- [38] P. Sarmah, R.C. Deka, *J. Mol. Model* 16 (2010) 411–418.
- [39] I. Fleming, *Frontier Orbitals and Organic Chemical Reactions*, Wiley, London, 1976.